

Figure Captions for supporting data

Fig. S1. XRD patterns of g-C₃N₄, CNTs, g-C₃N₄/Au, g-C₃N₄/CNTs and g-C₃N₄/CNTs/Au hybrids.

Fig. S2. Optical absorbance spectra of the colloidal dispersions of Au nanoparticles.

Fig. S3. BET surface areas calculated using nitrogen adsorption–desorption isotherms. (a) g-C₃N₄, (b) g-C₃N₄/Au formed using the 100-vol.% Au dispersion, (c) the g-C₃N₄/CNTs hybrid with a mass ratio of 60:40, and (d) ternary g-C₃N₄/CNTs/Au with a g-C₃N₄/CNTs mass ratio of 60:40 formed using the 100-vol.% Au dispersion. The insets show the corresponding pore-size distributions.

Fig. S4. XPS data for the ternary g-C₃N₄/CNTs/Au hybrid with a mass ratio of 60:40 and the 100-vol.% Au dispersion. (A) Survey scan and (B) high-resolution spectrum for C 1s, (C) high-resolution spectrum for N 1s, and (D) high-resolution spectrum of Au 4f.

Fig. S5. UV-vis absorption spectra for the photocatalytic degradation of RhB under irradiation with visible light using 50 mg L⁻¹ of the photocatalyst for g-C₃N₄, g-C₃N₄/Au, g-C₃N₄/CNTs and g-C₃N₄/CNTs/Au samples with 100 vol.% Au dispersions.

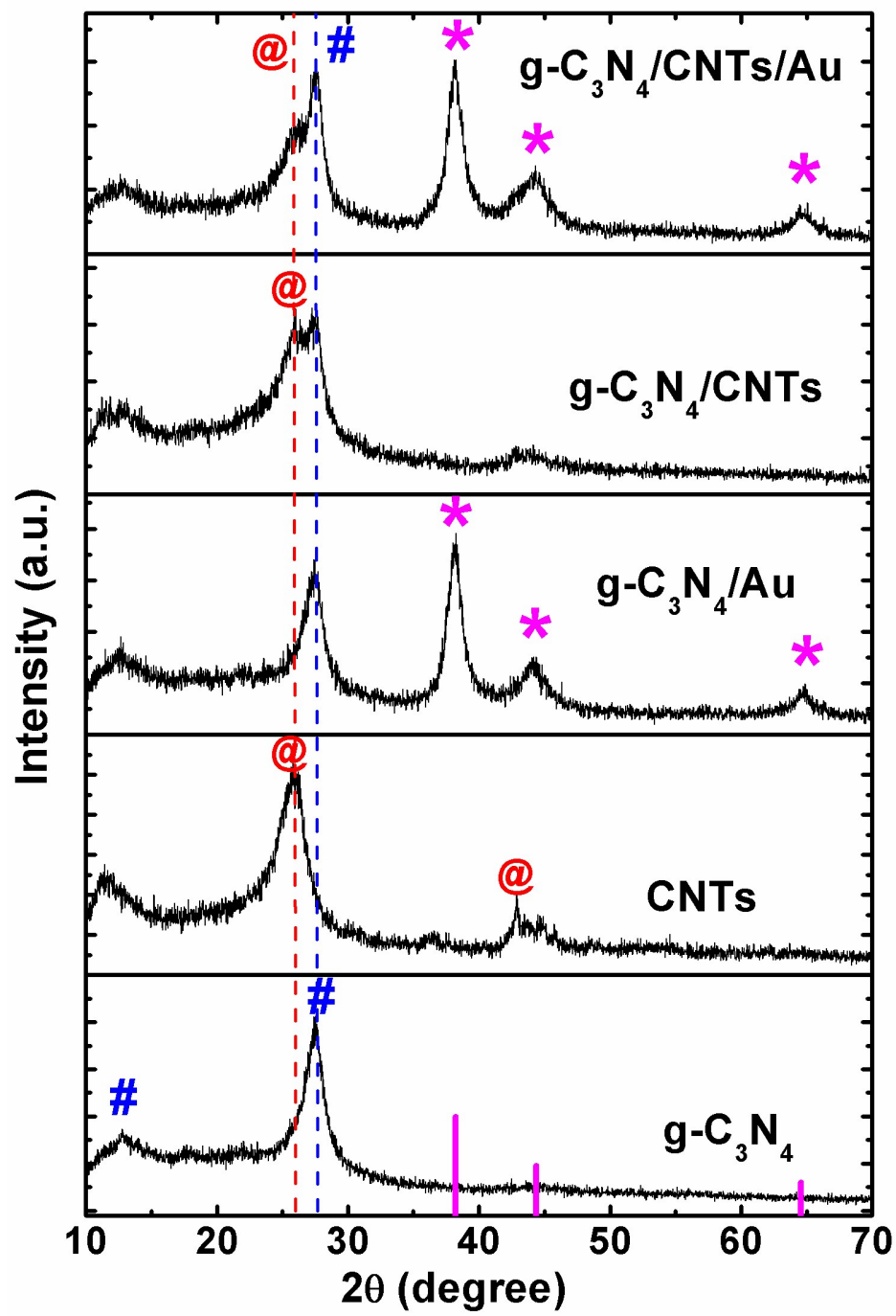


Figure S1

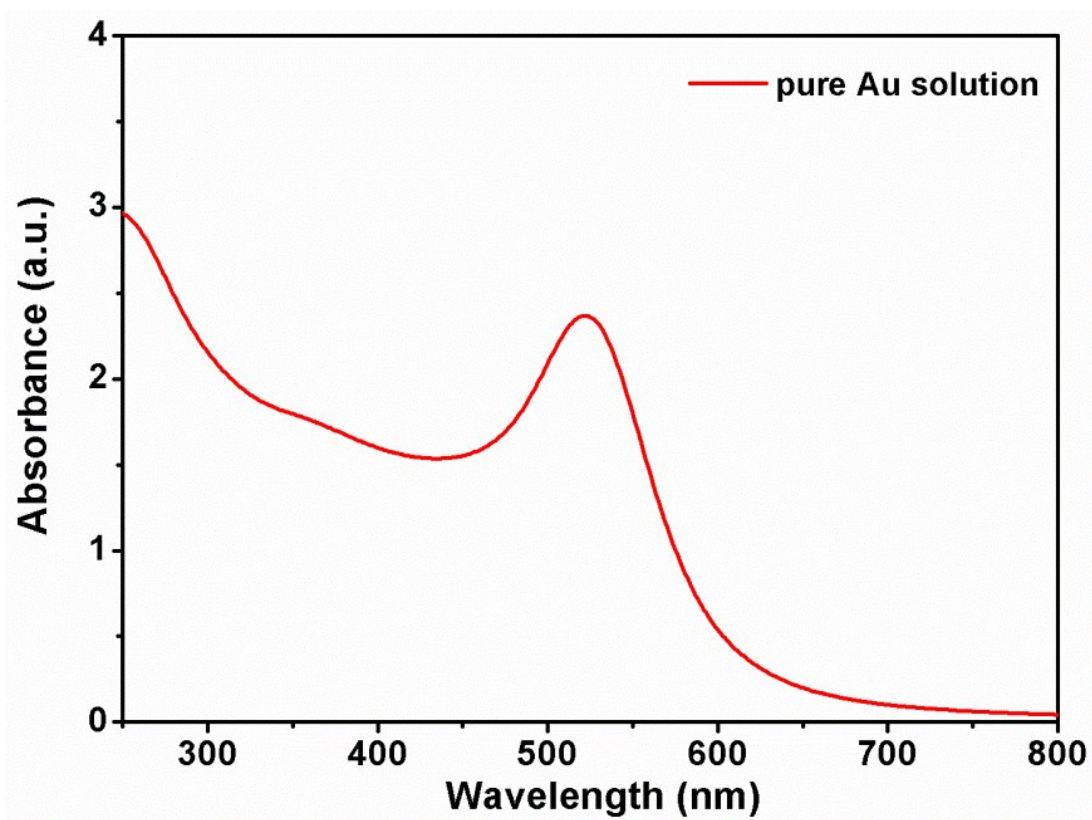
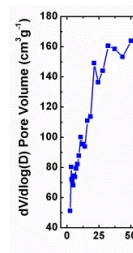
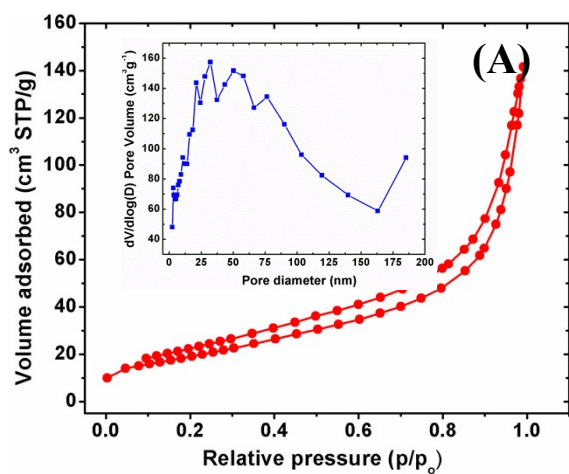
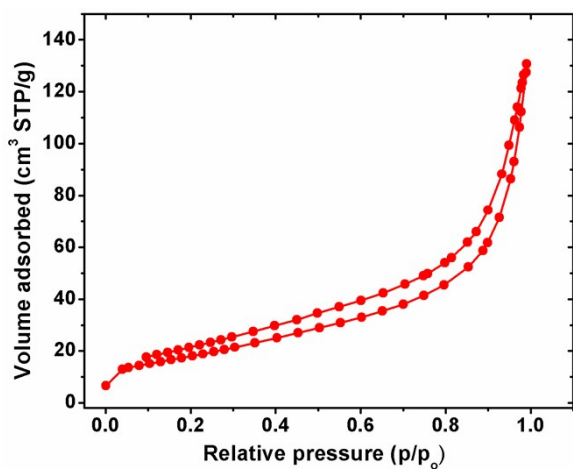


Figure S2



$= 71.02 \text{ m}^2\text{g}^{-1}$

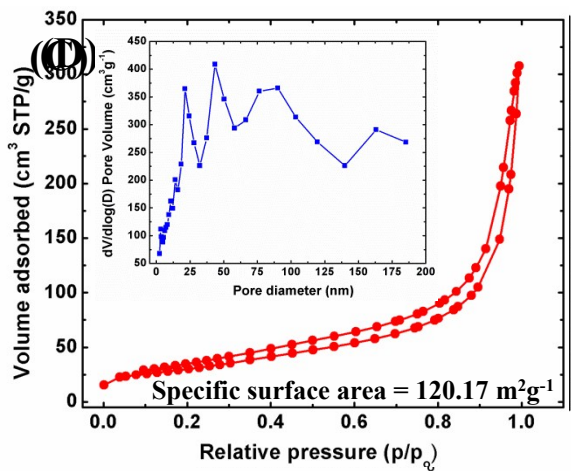


Figure S3(A to D)

N 1s

(C)

Au 4f

(D)

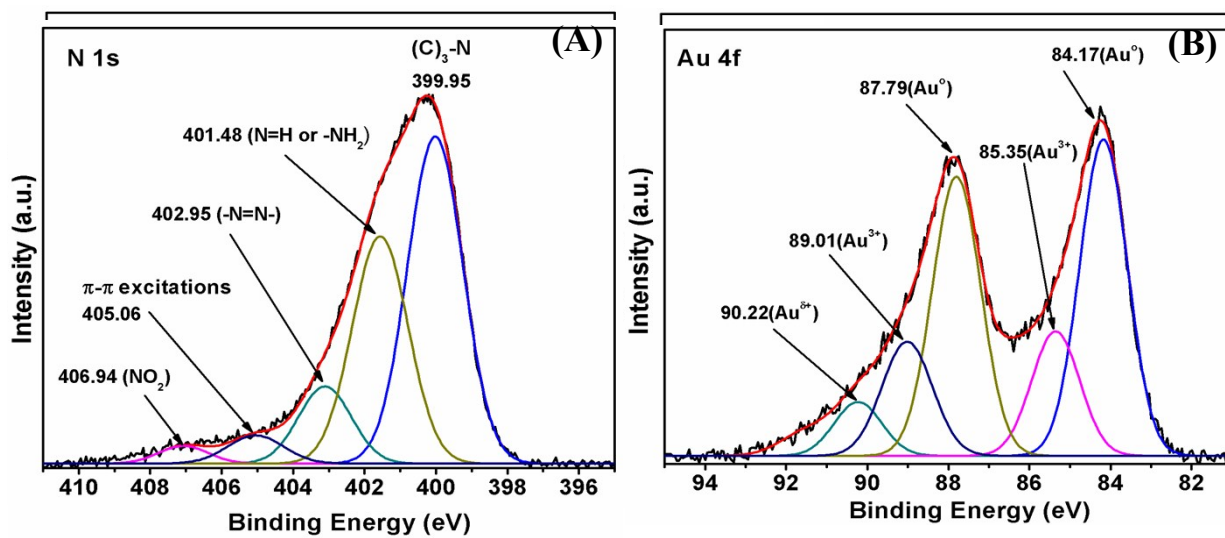


Figure S4(A-D)

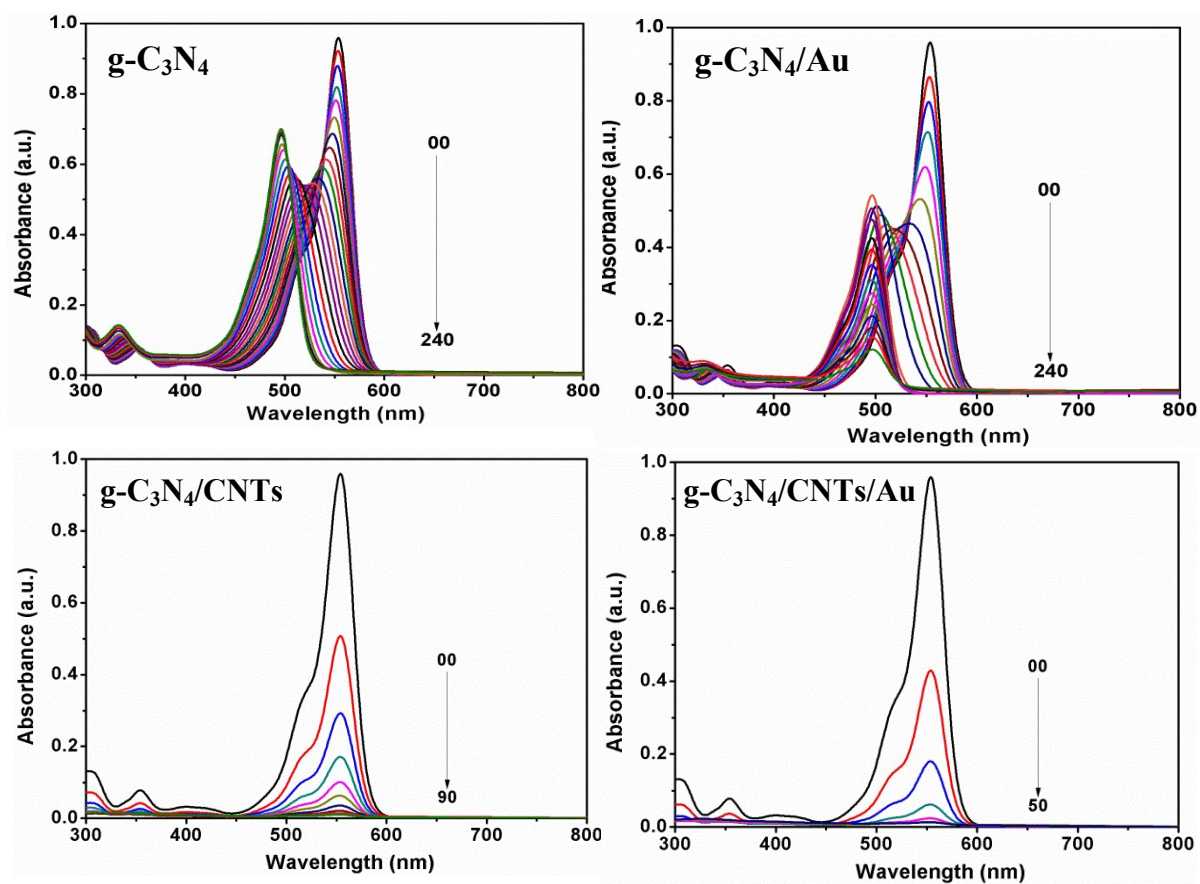


Figure S5